ISSN 2007-9737

Bioimpedance for Glucose Monitoring: Electrode Configuration and Metabolic Variability in Experimental Studies

Sebastián Yepes-Largo[1], Andrea Rodríguez-Lopez[2], Rene Antaño-López[1,*]

[1] Centro de Investigación y Desarrollo Tecnológico en Electroquímica, Mexico

[2] Universidad Politécnica de Santa Rosa Jáuregui, Mexico

rantano@cideteq.mx

Abstract. The search for non-invasive methods to estimate blood glucose levels has driven research into bioimpedance based on Electrochemical Impedance Spectroscopy (EIS) [1,2]. Various studies have demonstrated correlations between glucose levels and the electrical properties of the skin measured through impedance [3]. To enhance accuracy, optimizing factors such as electrode geometry is essential. This work investigated the configuration of contiguous parallel plate electrodes through simulations and experimental measurements in skin analog materials (SAM) and human skin. Measurements on three healthy volunteers, combining impedance and glucometry, examined glucose absorption and its effects on skin resistance. The results revealed impedance changes reflecting metabolic alterations induced by glucose, consistent with previous studies. Continuous measurements over 2.5 hours showed a probable correlation between impedance and blood glucose levels, albeit with a delay due to tissue differences, highlighting the complexity of the skin's response to glucose.

Keywords. Electrode geometry, skin impedance sensor, non-invasive method, skin resistance, resistivity-glucose correlation.

1 Introduction

Currently, diabetes is one of the leading causes of global mortality and is characterized by elevated blood glucose levels. To maintain homeostasis, the body involves both internal and external tissues, with the skin playing a crucial role in providing water and analytes. Glucose imbalances also affect other analytes in the skin, such as chloride (Cl^-) and sodium (Na^+), triggering associated diseases. Hypernatremia, characterized by elevated sodium levels, can result from dehydration due to polyuria related to diabetes, affecting neuronal function and water balance [4].

Conversely, hyponatremia, characterized by low sodium levels, may be caused by excess vasopressin due to hyperglycemia, leading to fluid retention and sodium dilution in the body [5]. These electrolyte imbalances are relevant in clinical management of diabetes. Sodium imbalances in the skin manifest in characteristic signs affecting its composition and metabolic activity in ionic exchange, resulting in dehydration and deterioration. Figure 1 illustrates the differences between diabetic skin and young, healthy skin.

Traditional glucose diagnosis and monitoring are performed through invasive techniques, which carry risks due to tissue intervention [7]. This has driven the development of non-invasive methods, such as Raman spectroscopy, reverse iontophoresis, and bioimpedance, which offer alternatives for disease management. Bioimpedance presents technical challenges, such as electrode placement and frequency range selection, which are essential for the accurate quantification of tissue electrical properties. Additionally, maintaining a stable state in biological systems during measurements is crucial. Studies have demonstrated that the stratum corneum, consisting of 15 to 20 layers of dead cells with a thickness of 10 to 40 μm, has a resistance of approximately 10^5 Ω·cm² and a capacitance of 30

nF·cm², playing a role in skin impedance, particularly in low-frequency ranges [8,9].

This work focuses on optimizing the surface electrode geometry for bioimpedance measurement using a 3-electrode configuration in skin analog materials (SAM).

Additionally, it explores the correlation between impedance measurements and glucose levels in volunteers with type 2 diabetes, a population in which non-invasive methods are particularly relevant due to the skin alterations they present, such as skin thickening and increased susceptibility to infections and wounds.

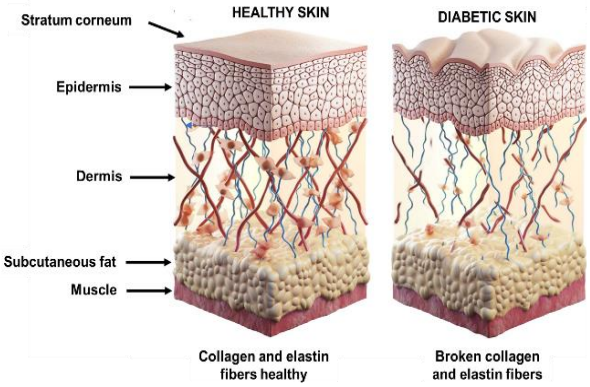

Fig. 1. Schematic illustration of changes in human skin related to diabetes. (Dremin et al., 2021) [6]

2 Methodology

To perform impedance measurements on SAM and human skin, we implemented a five-stage process. The first stage involved determining the appropriate geometry and constructing electrodes for impedance measurements using a three-electrode (3E) configuration. To achieve a meaningful approximation of biological tissue characteristics, SAM was fabricated using bovine skin gelatin (BSG) diluted with sodium chloride concentrations, following the concentrations reported in medical literature [10] to mimic sodium imbalances in blood. Subsequently, impedance measurements were conducted on volunteer skin using the previously constructed electrodes in the 3E configuration. Finally, the spectra obtained from SAM and volunteer skin were validated, and the results were analyzed.

2.1 Electrode Construction (3E)

For the construction of the electrodes, a 0.08 mm thick stainless steel 316 sheet was used. The sheets were cut into rectangles measuring 2.5 cm x 6.5 cm, using a prototype for piece cutting. Once cut, the pieces were assembled on 7.5 cm x 4.5 cm medical tape to avoid cross-contamination with conventional tape adhesives and to work with sterilized materials that would not affect the measurements. The use of medical tape allowed the skin to breathe through the micropores present in its structure, preventing the formation of air pockets that could affect impedance measurements.

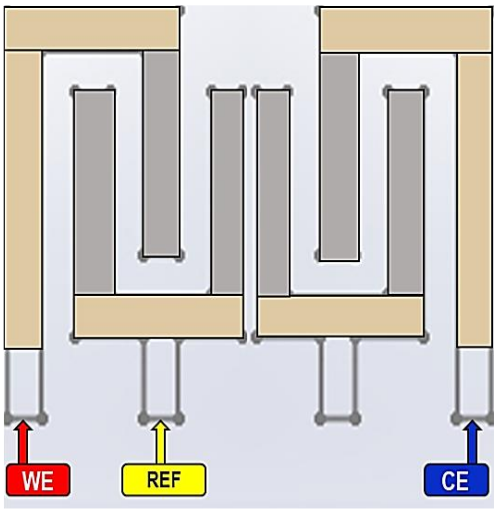

Fig. 2. Diagram for the 3E measurement device

Contact sites were limited to the rectangular areas between the electrodes in parallel plates on the skin surface, while other contacts were isolated with medical tape.

Factors influencing the geometry and construction of the 3E electrodes in a configuration of contiguous parallel plates included the optimization of the contact area between the electrode and the tissue, the reduction of interface resistance, the distribution of the electric field, and the adherence to biological tissue. Stainless steel 316 exhibits biocompatible properties that minimize the risk of adverse reactions and promote

safe interaction with biological tissues, contributing to the stability of the measurements.

2.2 Fabrication of Skin Analog Materials

In the fabrication of SAM, bovine skin gelatin (BSG) was used due to its ability to approximate human skin behavior. This gelatin contains collagen, a fibrous protein that makes up approximately 75% of skin and connective tissues in the human body [10]. Collagen is essential for the structure and function of the skin, providing strength and elasticity. Additionally, bovine skin gelatin serves as an appropriate matrix for mimicking the mechanical and biochemical properties of the skin due to its similar composition of water-soluble proteins with medium molecular weight. This makes it a good approximation for simulating skin conditions in experimental studies. Five types of SAM were prepared, with 8 g of agar diluted in 100 ml of deionized water. The details are summarized in the following table 1.

Table 1. Description and composition of the skin analog material, detailing the NaCl concentration and the characteristics of the gel used

SAM	CXN [NaCl]/M	Description	Composition
BLANK	0	Natural Resistance of SAM	8 g PBV + 100mLH_2O
PBV_HIPO	0.029	Low NaCl Concentration [52, 60]	
PBV_HIPO~ NORMO	0.038	Intermediate NaCl Concentration	
PBV_NORMO	0.055	Normal NaCl Concentration [52, 60]	
PBV_HIPER	0.088	High NaCl Concentration [52, 60]	

2.3 Impedance Measurements in Skin Analog Material

For the impedance measurements, a Solartron potentiostat (SI-1287) was used. This device performs electrochemical impedance measurements with a relative error of ±0.5% and a resolution of 0.1 μV. Calibration was carried out using a dummy cell and applying the electrochemical impedance technique with a potential of 0.1 V, considered optimal for this type of calibration. The device was configured in potentiostatic mode, and a three-electrode (3E) arrangement was used, applying a perturbation of 50 mV (70.7 mV RMS). This potential was validated through impedance measurements in the range of 10 to 90 mV, and the stability of the system was confirmed through voltametric tests.

Measurements were performed for a frequency range from 10 kHz to 10 mHz, capturing 8 points per decade while maintaining steady state during each test, which lasted 9 minutes. To reduce external noise, the system was isolated using a Faraday cage constructed from acetate and aluminum foil. The effectiveness of the cage was verified through external noise tests, electromagnetic field tests, perturbation tests, and visual analysis of light incidence. Detailed inspection of the impedance spectra, particularly at low frequencies, allowed for the characterization of the electrical parameters of the skin analog material (SAM), identifying resistive and capacitive contributions, suggesting a charge transfer process. The equivalent circuit used to model these measurements is shown in Fig. 3(a).

2.4 Simultaneous Impedance Measurements in Human Skin with Glucose Tolerance Testing

A pilot study was conducted to investigate the relationship between skin resistance and blood glucose levels, utilizing an experimental design with ten healthy volunteers aged between 25 and 30 years. Participants were selected based on strict exclusion criteria, including the absence of skin pathologies, use of pacemakers, pregnancy, large metal implants, and chronic diseases. Each volunteer was administered a saturated dextrose solution (75 g in 200 ml of H_2O), followed by glucose measurements every 40 minutes for 2.5 hours using a commercial glucometer, the Freestyle Optium from Abbott®. Simultaneously, volunteers were equipped with an impedance

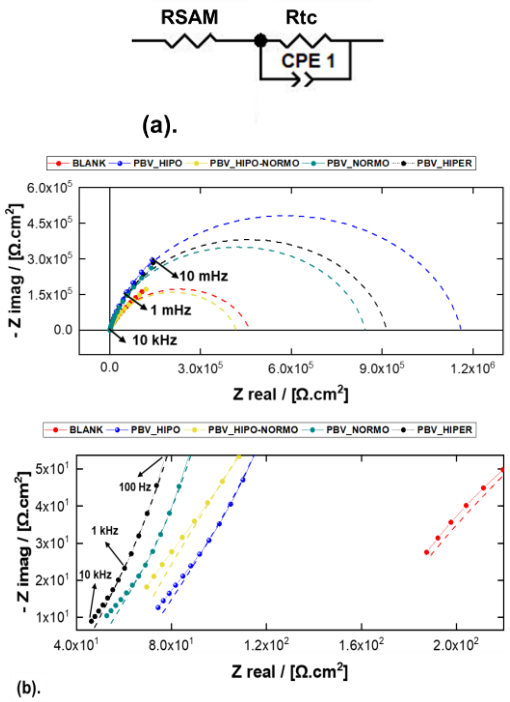

Fig. 3. (a) Equivalent Circuit for Impedance Testing in SAMs (b). Complete Nyquist plot (top right), and inset view at high frequencies of the Nyquist plot (bottom)

sensor placed on the forearm to evaluate changes in skin impedance. Impedance measurements were performed using a PalmSens4® potentiostat in potentiostatic mode, applying a potential of 50 mV (70.7 mV RMS). The accuracy of the PalmSens4® is determined by its ability to measure impedance with a typical error margin of ±1% within the measurement range. Calibration of the potentiostat was performed using a dummy cell, manufactured and provided with the device by PalmSens, applying the electrochemical impedance technique and utilizing a potential of 0.1 V, considered optimal for calibrating this device.

A frequency range of 10 kHz to 10 mHz was established, with 8 points per decade, and impedance spectra were recorded. An automated algorithm was implemented to schedule 5-minute measurement cycles consisting of 2.5 minutes of testing and 2.5 minutes of rest to minimize experimental interference and maintain the steady state of the skin tissue. The algorithm was designed with the help of a block programming script integrated into the PSTrace® software, which controls the PalmSens4® potentiostat, allowing for the establishment of time intervals between measurements. To manage experimental interference, patients were positioned in a supine position to avoid strain on the extremities or discomfort that could induce movements affecting the impedance measurement.

The reference electrodes of the measurement device underwent cathodic treatment involving the electrodeposition of chlorides on the silver surface, resulting in silver/silver chloride reference electrodes. All jewelry and shoes were removed from the patients, who were also instructed to wear sportswear during the measurements. Ambient temperature was maintained at 23 degrees Celsius to ensure the stability of bioimpedance measurements, as temperature variations affect the electrical conductivity of biological tissue and influence the results.

3 Results

3.1 Impedance Measurements in Bovine Skin Agar with Stainless Steel Electrodes in 3E Configuration

Impedance measurements conducted on various skin analog materials (SAMs) in a three-electrode (3E) configuration revealed significant variations in resistive and capacitive properties. The Nyquist plot in Fig. 3 demonstrates that the impedance spectra for all SAMs exhibit a leftward shift on the X-axis at high frequencies compared to the NaCl-free SAM (PBV_BLANCO). This shift indicates reduced resistance for SAMs containing NaCl, reflecting increased material conductivity at high frequencies.

The PBV_BLANCO SAM, without NaCl, shows considerable resistance and a non-ideal capacitive contribution. In contrast, the PBV_HIPO SAM, with low NaCl concentrations, exhibits decreased resistance, suggesting that lower NaCl concentrations enhance material conductivity. The PBV_NORMO SAM, with intermediate NaCl concentration, demonstrates moderate resistance and an inclination in the spectrum that reflects a blend of resistive and capacitive characteristics.

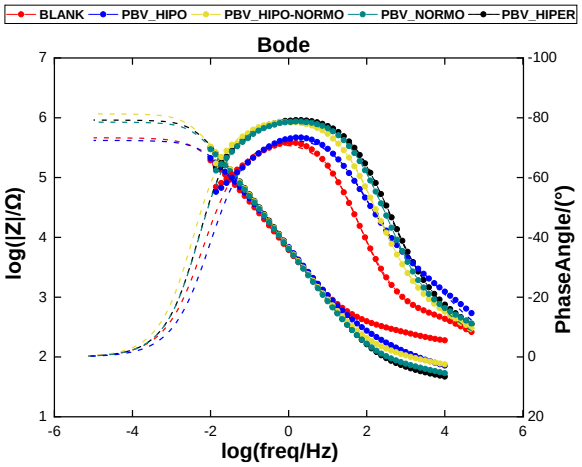

Fig. 4. Bode Phase and Bode Magnitude Plots for Impedance Measurements in Bovine Skin Agar for Dissolved NaCl Concentrations

Table 2. Values of RSAM, Rtc, and Capacitance Parameters for SAMs

Parameter	3E ELECTRODE CONFIGURATION				
	PBV_BLANCO	PBV_HIPO	PBV_HIPO~ NORMO	PBV_NORMO	PBV_HIPER
RSAM ($\Omega.cm^2$)	187.5	95.5	69.5	52.71	43.0
Rtc ($\Omega.cm^2$)	$8.1x10^5$	$1.1x10^6$	$4.2x10^5$	$1.0x10^6$	$9.1x10^5$
C_{eff} (F/cm^2)	9.8×10^{-5}	1.0×10^{-4}	9.3×10^{-5}	7.7×10^{-5}	1.0×10^{-4}

Table 3. Resistance Measurements of Skin Analog Materials with Different NaCl Concentrations

SAM	Measurement 1 RSAM ($\Omega.cm^2$)	Measurement 2 RSAM ($\Omega.cm^2$)	Measurement 3 RSAM ($\Omega.cm^2$)	Standard deviation ($\Omega.cm^2$)
BLANK	206.35	195.34	160.67	23.84
PBV_HIPO	79.91	84.71	58.46	13.98
PBV_HIPO~ NORMO	62.13	67.97	78.57	8.33
PBV_NORMO	52.86	49.21	56.06	3.43
PBV_HIPER	64.52	36.8	37.45	15.82

The PBV_HIPER SAM, with high NaCl concentrations, shows a pronounced leftward shift on the X-axis, indicating higher conductivity compared to PBV_BLANCO and other SAMs. This higher conductivity pattern is associated with the material properties influenced by the high NaCl concentration. Charge transfer characteristics of SAMs are affected by material composition, impurities, and drying processes. Table 2 lists the parameters for RSAM (resistance of SAM), Rtc, and capacitance obtained from impedance measurements.

Bode Phase and Bode Magnitude plots, shown in Fig. 4, complement the Nyquist plots and support the described equivalent circuit. They highlight the predominant resistive contributions at high frequencies across all five SAMs studied. In the Bode Magnitude plot, a parallel line to the X-axis at high frequencies represents RSAM for each scenario, followed by a line with a negative slope at intermediate frequencies, reflecting non-ideal capacitive contributions. At low frequencies, another parallel line to the X-axis indicates a resistive trend. The Bode Phase plot provides additional insight into low-frequency contributions, where all SAMs exhibit resistive contributions associated with charge transfer and non-ideal capacitive contributions, evident as a plateau in the spectra.

3.2 Reproducibility in Measurements of Skin Analog Gels

To evaluate the reproducibility of the measurements, three impedance measurements were conducted for each of the five experimental scenarios established for the skin-analog materials.

These repeated measurements validate the consistency of the sensor in estimating the resistance of the solution and minimize experimental variability. The results obtained are presented in Table 3 and demonstrate the capacity of the sensor to detect changes in resistance, considering the different concentrations of NaCl dissolved in the gels.

The data presented in Table 3 show the resistance measurements of the solutions across different experimental scenarios, along with their respective standard deviations. For the BLANK material, the resistance indicates considerable variability in the measurements. In the case of PBV_HIPO, the standard deviation reflects a moderate degree of reproducibility. For PBV_HIPO~NORMO, an improvement in measurement consistency is observed. Conversely, PBV_NORMO suggests high reproducibility in the estimation of the

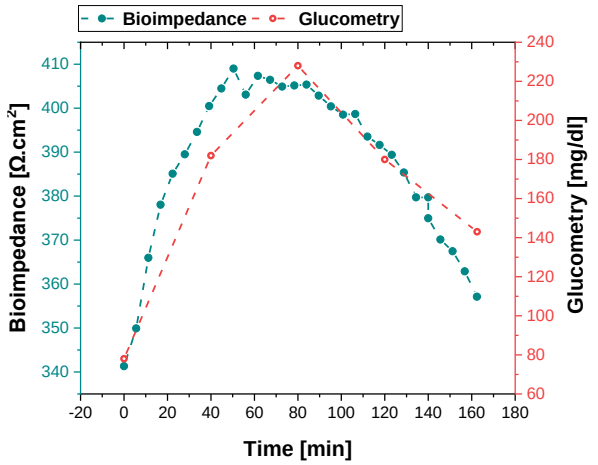

Fig. 5. Impedance Measurements in Human Skin in 3E Configuration vs. Glucometry

solution's resistance. Finally, PBV_HIPER presents significant variability, which may result from experimental factors or inconsistencies in the measurement process.

3.3 Impedance Measurements in Human Skin Concurrent with Glucose Tolerance Testing

Fig. 5 presents glucose meter measurements and impedance spectra obtained from the sensor, illustrating how skin resistance varies with blood glucose levels. The glucose meter readings show an initial increase in glucose concentration, followed by a decrease as endogenous insulin acts to restore balance. These variations are reflected in skin resistance values derived from 22 impedance spectra measured over 2.5 hours. The impedance spectra focused on characterizing the resistive and capacitive properties of the skin, showing that while no significant trends were observed in capacitive elements, resistance RSAM at 10 kHz exhibited a clear correlation with glucose changes. This finding suggests that skin resistance is a sensitive indicator of fluctuations in glucose concentration, enabling indirect monitoring of metabolic changes induced by glucose imbalances. The graph demonstrates how skin resistance changes align with blood glucose dynamics, showcasing the sensor's capability to consistently capture these variations.

4 Conclusions

Impedance measurements performed in a 3E configuration effectively identified changes in electrical properties of skin analog materials (SAMs) in response to varying NaCl concentrations, highlighting the system's ability to characterize bio-electrochemical materials under different ionic conditions. Additionally, glucose tolerance testing combined with impedance measurements revealed a correlation between blood glucose levels and changes in skin resistance. Impedance spectra showed variations in skin resistance due to metabolic imbalances induced by the glucose solution. These findings confirm the feasibility of the impedance sensor to effectively correlate glucose levels with changes in skin resistance, although a temporal delay in the skin's response was observed, indicating differences in the stabilization of external versus internal tissues.

References

1. **Huang, J., Zhang, Y., Wu, J. (2020).** Review of non-invasive continuous glucose monitoring based on impedance spectroscopy. Sensors and Actuators, A: Physical, pp. 311. DOI:10.1016/j.sna. 2020.112103.
2. **Martinsen, O.G., Heiskanen, A. (2023).** Bioimpedance and bioelectricity basics. Elsevier.
3. **Lin, T., Gal, A., Mayzel, Y., Horman, K., Bahartan, K. (2017).** Non-invasive glucose monitoring: A review of challenges and recent advances. Current Trends in Biomedical Engineering & Biosciences, Vol. 6, No. 5, pp. 1–8. DOI:10.19080/CTBEB.2017.06.555696.
4. **Resnick, L.M., Barbagallo, M., Gupta, R.K., Laragh, J.H. (1993).** Ionic basis of hypertension in diabetes mellitus: Role of hyperglycemia. American Journal of Hypertension, Vol. 6, No. 5, pp. 413–417. DOI: 10.1093/ajh/6.5.413.
5. **Zhang, Y., Li, C., Huang, L., Shen, X. (2021).** Relationship between hyponatremia and peripheral neuropathy in patients with

diabetes. Journal of Diabetes Research, DOI: 10.1155/2021/9012887.

6. **Dremin, V., Marcinkevics, Z., Zherebtsov, E., Popov, A., Grabovskis, A., Kronberga, H., Geldnere, K., Doronin, A., Meglinski, I., Member, S., Bykov, A. (2021)**. Skin complications of diabetes mellitus revealed by polarized hyperspectral imaging and machine learning. IEEE Transactions on Medical Imaging, Vol. 40, No. 4, pp. 1207–1216. DOI:10.1109/TMI.2021.3049591.
7. **Cinti, S., Arduini, F., Moscone, D., Palleschi, G., Gonzalez-Macia, L., Killard, A.J. (2015).** Cholesterol biosensor based on inkjet-printed Prussian blue nanoparticle-modified screen-printed electrodes. Sensors and Actuators B: Chemical, Vol. 221, pp. 187–190. DOI: 10.1016/j.snb.2015.06.054.
8. **Heikenfeld, J., Jajack, A., Rogers, J.A., Bond, J. (2018).** Wearable sensors: Modalities, challenges, and prospects. Lab on a Chip, Vol. 18 No. 2, pp. 217–248. DOI: 10.1039/c7lc00914c.
9. **Birgersson, O.S., Birgersson, E., Aberg, P., Nicander, I. (2010).** Non-invasive bioimpedance of intact skin: Mathematical modeling and experiments. Physiological Measurement, Vol. 32, No. 1, pp. 1–12. DOI: 10.1088/0967-3334/32/1/001.
10. **Hall, J.E. (2021)**. Guyton and Hall textbook of medical physiology. Elsevier.

Article received on 23/09/2024; accepted on 13/01/2025.
**Corresponding author is Rene Antaño-López.*